A role for quaternary structure in the substrate specificity of leucine dehydrogenase

Patrick J Baker*†, Andrew P Turnbull†, Svetlana E Sedelnikova, Timothy J Stillman and David W Rice

The Krebs Institute for Biomolecular Research, Department of Molecular Biology and Biotechnology, University of Sheffield, PO Box 594, Sheffield S10 2UH, UK

Background: Glutamate, phenylalanine and leucine dehydrogenases catalyze the NAD(P)$^+$-linked oxidative deamination of L-amino acids to the corresponding 2-oxoacids, and sequence homology between these enzymes clearly indicates the existence of an enzyme superfamily related by divergent evolution. We have undertaken structural studies on a number of members of this family in order to investigate the molecular basis of their differential amino acid specificity.

Results: We have solved the X-ray structure of the leucine dehydrogenase from *Bacillus sphaericus* to a resolution of 2.2 Å. Each subunit of this octameric enzyme contains 364 amino acids and folds into two domains, separated by a deep cleft. The nicotinamide ring of the NAD$^+$ cofactor binds deep in this cleft, which is thought to close during the hydride transfer step of the catalytic cycle.

Conclusions: Comparison of the structure of leucine dehydrogenase with a hexameric glutamate dehydrogenase has shown that these two enzymes share a related fold and possess a similar catalytic chemistry. A mechanism for the basis of the differential amino acid specificity between these enzymes involves point mutations in the amino acid side-chain specificity pocket and subtle changes in the shape of this pocket caused by the differences in quaternary structure.

Structure 15 July 1995, **3**:693–705

Key words: amino acid dehydrogenase superfamily, leucine dehydrogenase, quaternary structure, substrate specificity

Introduction

The oxidative deamination of amino acids to their corresponding keto acids is of central importance in metabolism and is catalyzed by the family of amino acid dehydrogenases. These enzymes also provide an important route for the incorporation of ammonia into organic compounds and link the metabolism of carbohydrates and amino acids. Leucine dehydrogenase (LeuDH) (E.C. 1.4.1.9) catalyzes the reversible oxidative deamination of L-leucine to 2-ketoisocaproate, with the corresponding reduction of the cofactor NAD$^+$:

$$\text{leucine}+\text{NAD}^+ + \text{H}_2\text{O} \leftrightarrow \text{NADH} + \text{NH}_4^+ + \text{H}^+ + \text{2-ketoisocaproate}$$

LeuDH was first isolated from *Bacillus cereus* [1] and has been characterized in many *Bacillus* species [2], where it functions in the catabolism of branched-chain amino acids. The preferred substrate is always leucine. However, other amino acids, such as valine and isoleucine, are also accepted by the enzyme [3].

The LeuDHs from *B. stearothermophilus* [4] and *Thermoactinomyces intermedius* [5] have been cloned and sequenced and contain 429 and 366 amino acids, respectively. A comparison of their amino acid sequences shows that the additional residues in the *B. stearothermophilus* enzyme form an extension at the C terminus. Sequence alignment studies have revealed the existence of strong sequence similarity between LeuDH and phenylalanine dehydrogenase (PheDH; 50% identical) and a somewhat more remote similarity to glutamate dehydrogenase (GluDH; 20% identical), indicating the existence of an enzyme superfamily with differential substrate specificity [4,6]. Homology-based modelling studies have shown that when the sequences of LeuDH and PheDH are mapped onto the three-dimensional structure of GluDH, the secondary-structure elements in the core of the two domains of GluDH appear to be conserved, and that residues implicated in catalysis are preserved [7]. Conversely, a small number of point mutations are found in the substrate side-chain-binding pocket which are thought to account for the differences in substrate specificity.

The quaternary structure of LeuDH has been reported as hexameric with subunit molecular weight 41 000 Da for the *B. sphaericus* strain IFO3525 [8]. However, electron microscopy studies indicate that LeuDH from *B. cereus* is an octamer with 42 symmetry and a subunit molecular weight of ~40 000 Da [9]. The LeuDH from *B. sphaericus* strain ATCC4525 has been purified, crystallized and shown to have a relative molecular mass of 41 000 by polyacrylamide gel electrophoresis [10]. Analysis of a self-rotation function calculated on a preliminary data set has shown that the quaternary structure for this enzyme is that of an octamer arranged in 42 symmetry [10]. This contrasts with the hexameric structure seen in GluDH and is consistent with the location of the major insertions and deletions in the aligned sequences of GluDH and LeuDH which are found near the threefold axis of GluDH [7].

*Corresponding author. †PJB and APT contributed equally to this work.

 ISSN 0969-2126

In this paper we report the structure of the LeuDH from *B. sphaericus*, strain ATCC4525. The structure reveals the molecular basis of the substrate specificity, identifies residues lying in the catalytic site, defines the features responsible for the differences in quaternary structure between LeuDH and GluDH, and suggests a role for the change in quaternary structure in substrate recognition.

Results

Structure determination

Crystals of LeuDH belong to space group I4, with a dimer in the asymmetric unit [10]. As no DNA sequence is yet available for the LeuDH from *B. sphaericus*, the model has been constructed using a combination of the sequence for the N-terminal 47 residues, derived from protein sequencing, together with a consensus sequence from *B. stearothermophilus* and *T. intermedius* LeuDHs. At the C terminus there is no sign in the electron-density map of an extension in the sequence similar to that found in *B. stearothermophilus* LeuDH, thus we assume that the sequence for the *B. sphaericus* enzyme is of a similar length to that of the *T. intermedius* enzyme although, at present, we cannot discount the possibility of there being additional residues at the C terminus which are disordered in the electron-density map. In certain places in the model the electron-density map indicates that neither the *B. stearothermophilus* nor the *T. intermedius* sequence is correct and in these positions we have selected a residue type that is the best fit to the observed electron density. At the surface of the protein this protocol must inevitably lead to considerable sequence errors, as the electron density for residues such as glycine, alanine and serine will be indistinguishable from weak electron density features associated with disordered residues. The sequences of the LeuDHs from *B. stearothermophilus*, *T. intermedius* and the final X-ray model sequence of the *B. sphaericus* enzyme are aligned with the GluDH from *Clostridium symbiosum* in Figure 1. In the final *B. sphaericus* LeuDH model 57 residues are different from those found in either the *B. stearothermophilus* or *T. intermedius* LeuDHs.

The LeuDH molecule

The LeuDH subunit is constructed from 14 α-helices and 12 β-strands, which comprise some 75% of the polypeptide chain. The secondary-structure assignments are given in Figure 1 and a schematic stereo representation of the structure of a single subunit of LeuDH is shown in Figure 2. The secondary-structure elements fold into two domains, separated by a deep cleft. Domain I consists of residues 1–136 and 332–364 and is composed of a mixed parallel/antiparallel β-sheet of six strands (βa–βf), flanked on each side by two α-helices (α1,α2 and α3,α4). A short helix (α5) joins the last strand of domain I (βf) with the long α-helix (α6) which leads into domain II. This domain (residues 137–331) resembles the classical dinucleotide-binding domain and folds into a central six-stranded parallel

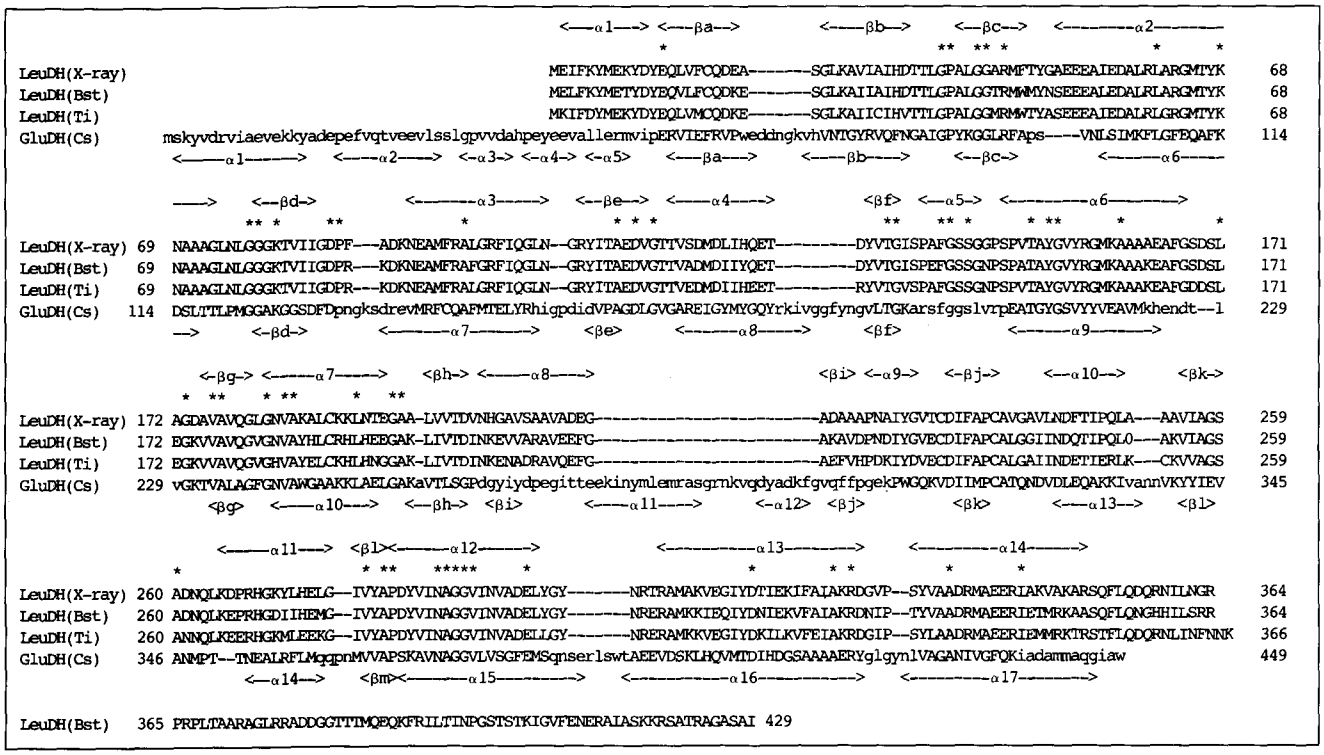

Fig. 1. Structure-based sequence alignment of the X-ray sequence of the LeuDH from *B. sphaericus* (X-ray), together with the sequences of the LeuDHs from *B. stearothermophilus* (Bst) and *T. intermedius* (Ti) and the GluDH from *C. symbiosum* (Cs). The residues of GluDH shown in upper case correspond to regions where the structures of GluDH and LeuDH are closely related. Residues identical in all four sequences are highlighted by an asterisk. Secondary-structure elements for LeuDH are shown above the sequences and those for GluDH below.

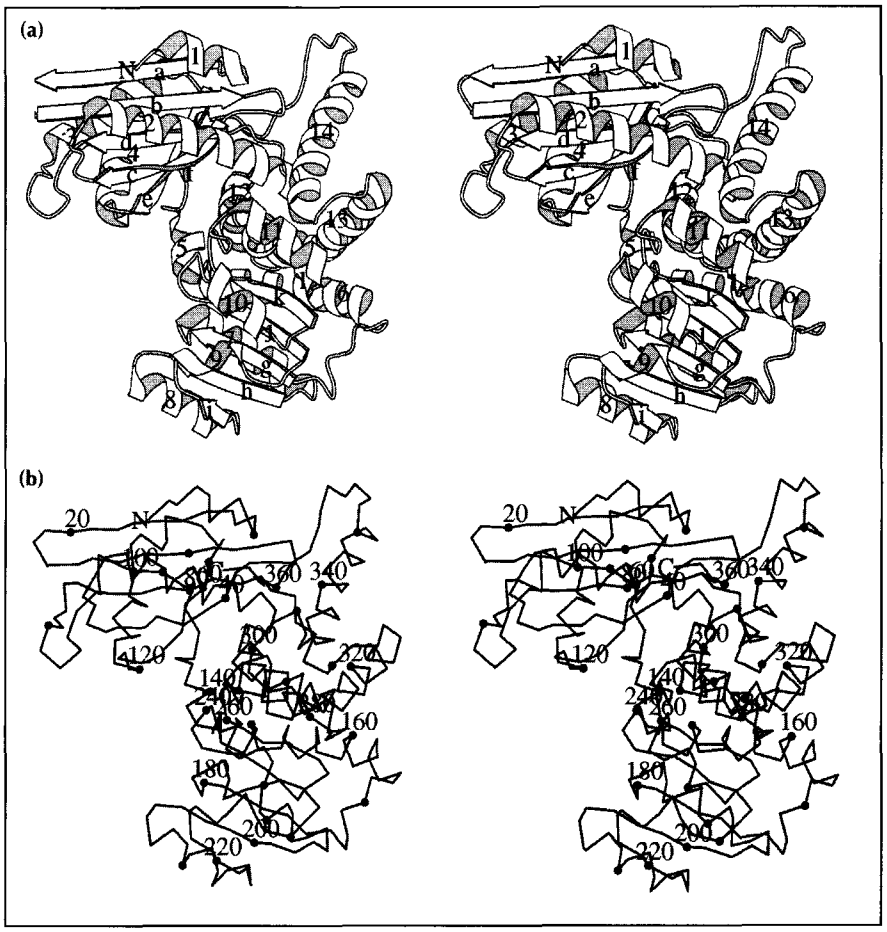

Fig. 2. Stereo diagrams of a single subunit of LeuDH. The organization of the subunit into two domains, separated by a deep cleft, can be seen. In this view the fourfold axis of the LeuDH octamer runs vertically. **(a)** Schematic representation with the strands and helices numbered. **(b)** Cα trace with every tenth residue indicated by a black dot. (Figure prepared using MOLSCRIPT [41].)

β-sheet (βg–βl) flanked on each side by two helices (α7,α8 and α10,α11). A short helix (α9) is present between strands βi and βj. The last strand of domain II (βl) is followed by helix α12 and a long helix, α13, which together with α6 dominate the domain interface and provide most of the interactions between the two domains. The subunit is completed by a further long α-helix (α14), part of which packs against the surface of the N-terminal domain, and an extended loop formed by the C-terminal 15 residues. The end of α14 and part of the C-terminal loop (residues 343–360) protrude somewhat from the surface of domain I, before folding back into the domain with the C terminus lying close to the end of α12. Two of the 14 α-helices (α12 and α13) contain 3_{10}-turns, formed by residues 287–289 and 311–313, respectively.

Quality of the model

The quality of the electron density and model is generally good, although it does vary somewhat throughout the model with the best-defined areas being the N-terminal domains of the two subunits (A and B) in the asymmetric unit. This is confirmed by the average main-chain B-factors, which are 28.1 Å^2 and 21.6 Å^2, for domain I of subunits A and B, respectively and 49.1 Å^2 and 63.0 Å^2 for domain II. Although the B-factors for the C-terminal domains of both subunits are somewhat high, the quality of the electron density for this domain in subunit A is such that we are confident that no ambiguity remains in the chain connectivity. This is confirmed by extensive OMIT map calculations which give no indication of alternative connectivities. Furthermore, all non-glycine residues for both subunits fall into the allowed regions of a Ramachandran plot. This general difference between the temperature factors of the two domains is a phenomenon that we have observed in all our crystallographic studies on members of the amino acid dehydrogenase superfamily, in numerous space groups and even at high resolution ([11,12]; ISB Abeysinghe and ML Waugh, unpublished data). In each case, unusually high B-factors are found for the C-terminal domains, which nevertheless are associated with interpretable density. As it is known that the two domains can adopt widely different conformations, which are related to the enzyme's catalytic cycle, one possibility is that the high temperature factors may arise from static disorder in the crystal. Particularly weak areas of electron density, common to both subunits in LeuDH, include the loop joining helices α5 and α6, which forms the junction between the two domains (144A–146A and 141B–146B), and the loop at the bottom of domain II at the periphery of the subunit, linking helix α6 with strand βg (166A–168A and 166B–175B). The electron density for domain II in subunit B is of poorer quality than that for subunit A. Nevertheless, it is not as poor as might be suggested by the high temperature factors, although the differences seen here, particularly in subunit B are higher than have been observed previously. These high

temperature factors for domain II in subunit B partly arise from an accumulation of a series of additional weak areas in the electron density which have no counterpart in subunit A and include the loop between α7 and βh (195B–198B), the N termini of α8 and α10 (206B–210B and 244B–247B, respectively), and the C terminus of α13 (321B–325B).

Quaternary structure

Eight LeuDH monomers fold into an octamer with 42 symmetry, which has a cuboid appearance and dimensions of 100 Å along the fourfold axis and an edge of 120 Å. A solvent channel runs through the entire molecule along the fourfold axis, with a maximum radius of 21 Å at the exterior of the molecule and minimum radius of 8 Å at the 42 symmetry point (Fig. 3). This overall molecular shape is in excellent agreement with small-angle X-ray scattering studies on *B. sphaericus* LeuDH, which indicated that the multimer was a hollow cylinder of 47 Å outer radius, 10 Å inner radius and length 133 Å, despite the prediction that the molecule was a hexamer [8]. Similarly, the channel along the fourfold axis was predicted from electron micrograph images of *B. cereus* LeuDH [9].

The majority of the interactions between the eight subunits in LeuDH come from residues in domain I, which interact both across the twofold axis to form dimers, as well as around the fourfold axis to assemble the octamer. These N-terminal domains form a compact core of the oligomer, with the eight C-terminal domains lying furthest from the 42 symmetry point and appearing in a staggered conformation when viewed down the fourfold axis (Fig. 3a). The dimer interface consists mainly of three interacting complementary areas. Centrally, strand βa (residues 11A–21A) interacts with its symmetry mate βa′ (11B–21B) across the twofold axis, in an antiparallel manner to form a sheet of 12 strands, perpendicular to the fourfold axis and spanning both subunits. On one side of this sheet the C-terminal end of α3 (residues 106 and 107) packs against the same residues in its twofold-related mate, with the methylene groups of the side chain of Arg109A making hydrophobic interactions with Phe102B. On the other side of this central sheet the interactions across the twofold axis are made up from one face of α1 from subunit A packing against residues 19B–26B. The main-chain amide groups of Met1A and Ile3A form hydrogen bonds with the side chains of Glu52B and Glu51B, respectively and the side

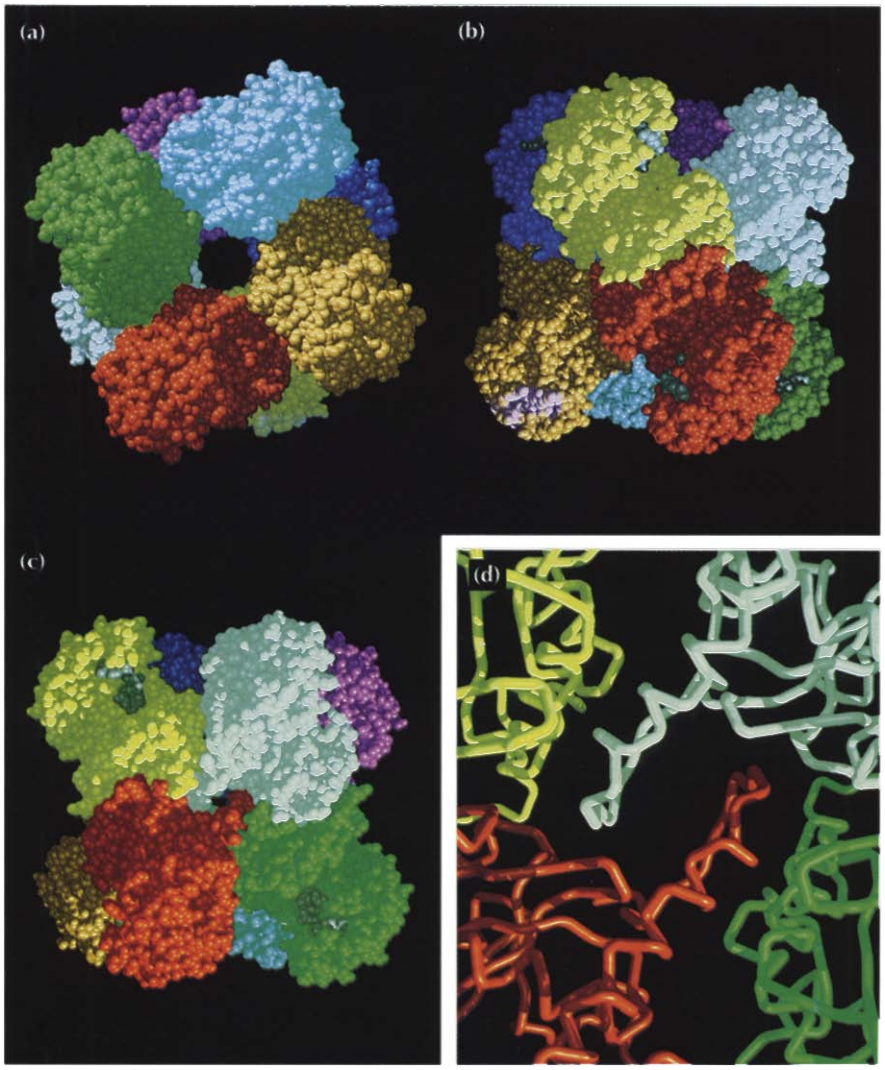

Fig. 3. Space-filling representations of the LeuDH octamer with each subunit individually coloured. **(a)** View down the crystallographic fourfold axis. **(b)** View down the non-crystallographic twofold axis used to construct the dimer, with the fourfold axis vertical. The bound NAD^+ moieties can be seen in dark green, with the nicotinamide ring deep in the cleft between the two domains. **(c)** The octamer viewed down the non-crystallographic twofold axis which relates pairs of dimers, with the fourfold axis vertical. The association of the subunits across this axis can be seen. **(d)** Close-up ribbon diagram of view (c). Two dimers are shown, AB (red and yellow) and A′B′ (green and white). The C-terminal helix and loop of subunits A and B′ can be seen to come together around this twofold axis, forming a 'handshake' between the two dimers. (Figure prepared using Midas Plus [42,43].)

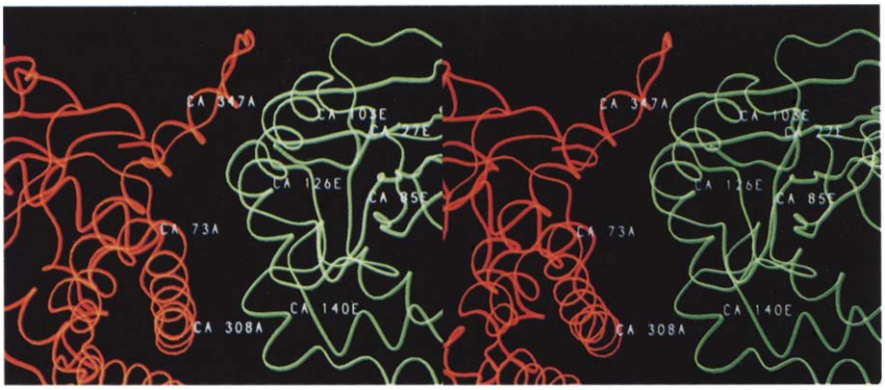

Fig. 4. Stereo ribbon diagram illustrating the interactions around the fourfold axis in LeuDH. Two monomers are shown (red and green), viewed down the non-crystallographic twofold axis which relates pairs of dimers, with the fourfold axis vertical. (Figure prepared using FRODO [38].)

chain of Phe4A packs in a hydrophobic pocket formed by Ile84B and the methylene groups of the side chains of Lys26B and Glu51B.

To describe the interactions made between the four dimers around the fourfold axis we define the subunits which lie in one square-planar ring as A, A′ and so on, and their twofold-related partners as B, B′ and so on, The interface around the fourfold axis is composed of a concave face on subunit A, formed from α13, the α2–βd loop, α12 and the α11–α12 loop, packing against a convex face on subunit A′, formed by the βa–βb loop, the βd–α3 loop, α3, α4 and the loop to βf and α5 (see Fig. 4). Furthermore, the end of the C-terminal helix (α14) and the loop to the C terminus form a protruding arm from one subunit (A), which slots into a complementary U-shaped pocket some 15 Å deep and 8 Å wide, constructed from residues in both subunits of the neighbouring dimer (A′B′; Fig. 3). Specifically, one face of the pocket is made from the βa–βb loop, α3 and α4 from subunit A′; the base of the pocket is made from the βb–βc and α3–βe loops from subunit B′ and the other face is built from the C-terminal helix (α14) and C-terminal loop, also from subunit B′. Thus, the C-terminal arms from two subunits form a 'handshake' around the twofold axis which relates dimers (Fig. 3d). Along this axis, a channel measuring some 8×4 Å leads to the interior of the molecule (Fig. 3c). The character of the fourfold interface is mainly hydrophilic, with hydrogen bonds formed between Asn75A–Gln128A′, Asn75A–Arg97A′, Tyr299A–Gln128A′, Arg342A–Glu93A′, Arg350A–Glu129A′, Asp356A–Asn107B′, Asp356A–Gln104A′, Gln357A–Arg101A′, Arg358A–Asp131A′ and Arg358A–Thr130A′. This interface is completed with the side chain of Phe353A stacking against the ring of Pro38B′. Of these 18 residues, 11 are identical in the *B. stearothermophilus* and *T. intermedius* LeuDH sequences, with a further four being conservatively substituted.

Surface accessible areas for an individual subunit, an AB dimer, a tetramer of four A subunits and the complete octamer of LeuDH have been calculated by the method of Lee and Richards [13]. A single subunit of LeuDH possesses a surface area of 16100 Å^2. On forming an octamer, 21.3% of the subunit surface area is buried, with 1250 Å^2 (7.9%) being buried at the twofold axis, 1550 Å^2 (9.7%) at the fourfold axis and 600 Å^2 (3.7%) on formation of the octamer.

Discussion

Similarity to GluDH

We have previously predicted [7], on the basis of a structure-based sequence alignment, that the three-dimensional structure of LeuDH would share many common features with that of GluDH, the only other amino acid dehydrogenase whose structure is known [11]. When these two structures are compared it is seen that they do indeed share a similar folding pattern and domain organization. The areas of greatest similarity lie packed in the core of the subunit, with the differences restricted to more exposed regions. GluDH has 59 and 26 extra residues in domains I and II, respectively, relative to LeuDH and these lead to minor differences in topology. More importantly, however, they create significant changes in the subunit interface regions which result in modifications to the quaternary structure. In the following discussion the numbers of the secondary-structure elements are those relating to LeuDH (the equivalent secondary-structure elements and residue numbers for GluDH are shown in Fig. 1).

The first stretch of sequence and structural similarity between LeuDH and GluDH occurs at the start of βa. N-terminal to this, the first 16 residues in LeuDH fold into a single α-helix, whereas in GluDH the first 54 residues fold into a subdomain of five helices on the periphery of domain I. None of the helices in GluDH share the same position as α1 in LeuDH.

In LeuDH, domain II folds into a structure similar to that seen in the classical nucleotide-binding domain of lactate dehydrogenase, as described by Rossmann *et al.* [14,15]. In contrast, the folding pattern of the nucleotide-binding domain in GluDH, although highly reminiscent of LeuDH, is different, with the direction of one of the strands reversed and an extra strand and helix being present (Fig. 5). These differences are located between strands βh and βj in LeuDH (residues Asn205–Ile226), a region where no sequence homology can be detected between the two enzymes and where a 25-residue insertion is present in GluDH. Indeed, the extremities of the

nucleotide-binding fold are, in general, poorly conserved throughout the dehydrogenase family [16–18]. For example, two extra strands are present at this position in glyceraldehyde 3-phosphate dehydrogenase [19].

A major difference between LeuDH and GluDH is in quaternary structure, with these enzymes adopting octameric and hexameric assemblies, respectively. Around the twofold axis, LeuDH and GluDH share a very similar structure. In both enzymes the sheet in domain I continues across the twofold axis to form a 12-stranded sheet. However, the orientation of this sheet differs with respect to the fourfold or threefold axis. In LeuDH, strands βa and βa′ lie approximately perpendicular to the fourfold axis, whereas in GluDH these strands make an angle of some 32° to the threefold axis, which arises in part from the relative tilt of the dimers with respect to the fourfold or threefold axes in the two structures (Fig. 6a,b).

In contrast, the assembly of the dimers into their respective multimers is quite different in LeuDH and GluDH. There are five segments of polypeptide chain where sequence differences and insertions or deletions between LeuDH and GluDH are present which have profound implications for oligomer formation (Fig. 4). Four of these regions involve interactions around the threefold axis in GluDH [7]. Compared with GluDH, the loops between βa–βb and α3–βe in LeuDH are seven and five residues shorter, respectively. Furthermore, the α4–βf and α12–α13 loops are shorter, with both α4 and α12 also losing a turn at their C termini, resulting in nine and six residue deletions in these areas for LeuDH. Lastly, in GluDH the C-terminal residues (424–449) form a helix that packs against the helical subdomain formed by the first 54 residues in domain I and is not involved in the oligomeric assembly. In contrast, in LeuDH residues 331–350 form a helix which is oriented differently and which is followed by the C-terminal loop, with both these elements forming important interactions across the fourfold axis. These sequence differences, involving both residues important for the threefold assembly in GluDH and also the fourfold assembly in LeuDH, explain the different modes of association of the dimers in these two enzymes (Fig. 6c,d). Despite these differences, the overall structure of the subunits of GluDH and LeuDH is remarkably similar. If the two subunit structures are superimposed, the α-carbon atoms of domains I agree with a root mean square (rms) deviation of 1.25 Å (104 residues compared), and those in domains II agree with an rms deviation of 1.85 Å (121 residues compared).

Dinucleotide binding

In order to establish the location of the dinucleotide-binding site of LeuDH we collected 2.5 Å data on a crystal soaked in 3 mM NAD^+. Difference Fourier analysis showed a single strong electron density feature associated with subunit A, into which an NAD^+ moiety could be built (Fig. 7a). No density was observed for subunit B. In an attempt to view the binding of the cofactor to subunit B, we also soaked crystals in higher concentrations of NAD^+, but in all cases the crystals cracked. As the environments and conformations of the two subunits are different in the crystal, there are presumably minor differences in binding affinities for NAD^+ in each subunit, with the concentration required for NAD^+ to bind to subunit B being higher than that for subunit A. The disintegration of the crystals at higher NAD^+ concentrations is presumably linked to conformational changes associated with NAD^+ binding to subunit B causing destabilization of the crystal lattice. For subunit A, the map indicated that, upon cofactor binding, movements occur in the LeuDH main chain in the βg–α7 loop (residues 180–183) and also at the N terminus of helix α6 (residues 147–150) together with reorientations of certain side chains to optimize the interactions of the enzyme with the cofactor (Fig. 7b). The quality of the map allowed unambiguous positioning of the adenine ring, the identification of the C2′-*endo* conformation for both ribose rings, the clear definition of the backbone phosphates and the assignment of a *syn* conformation for the glycosidic bond linking the nicotinamide ring and its associated ribose.

The precise interactions between the enzyme and the dinucleotide, and details of the movements of the protein main chain, require the structure of this binary complex to be refined at high resolution. Nevertheless, this preliminary study has allowed us to determine the nature of the enzyme–cofactor interactions (Fig. 7b). As has been observed in many dehydrogenases [20], the adenine ribose hydroxyl groups make specific hydrogen bonds to

Fig. 5. Stereo ribbon diagram of the superimposed dinucleotide-binding domains of LeuDH (orange) and GluDH (blue). Between residues 204 and 226 in LeuDH the polypeptide chain adopts a 'classical' dinucleotide-binding fold, in contrast to GluDH in which extra elements of secondary structure are present. (Figure prepared using FRODO [38].)

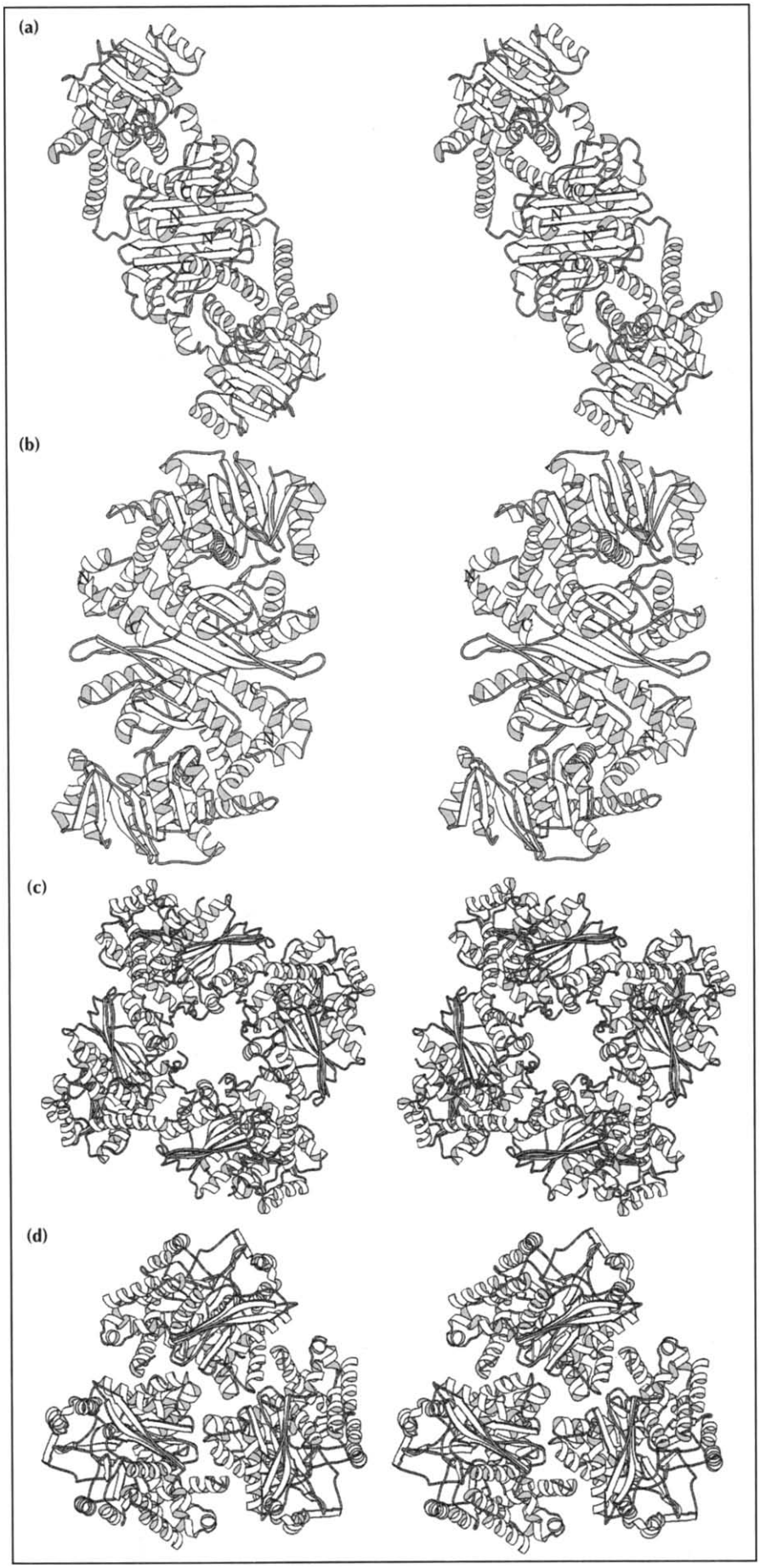

Fig. 6. Stereo representations of the dimers of **(a)** LeuDH and **(b)** GluDH, viewed down their respective dimer twofold axes, with the fourfold axis in LeuDH and the threefold axis in GluDH vertical. The close similarity in secondary structure and domain organization between these two enzymes can be seen. The central β-sheet that extends across the N-terminal domains of LeuDH is approximately perpendicular to the fourfold axis, whereas in GluDH the equivalent sheet is rotated by some 32°, approximately corresponding to the relative rotation of the dimers. **(c)** The tetramer of LeuDH viewed from the 42 symmetry point down the fourfold axis. **(d)** The trimer of GluDH viewed from the 32 symmetry point down the threefold axis. The differences in association of the LeuDH and GluDH subunits around their fourfold and threefold axes contrasts with the similar mode of assembly of their dimers. (Figure prepared using MOLSCRIPT [41].)

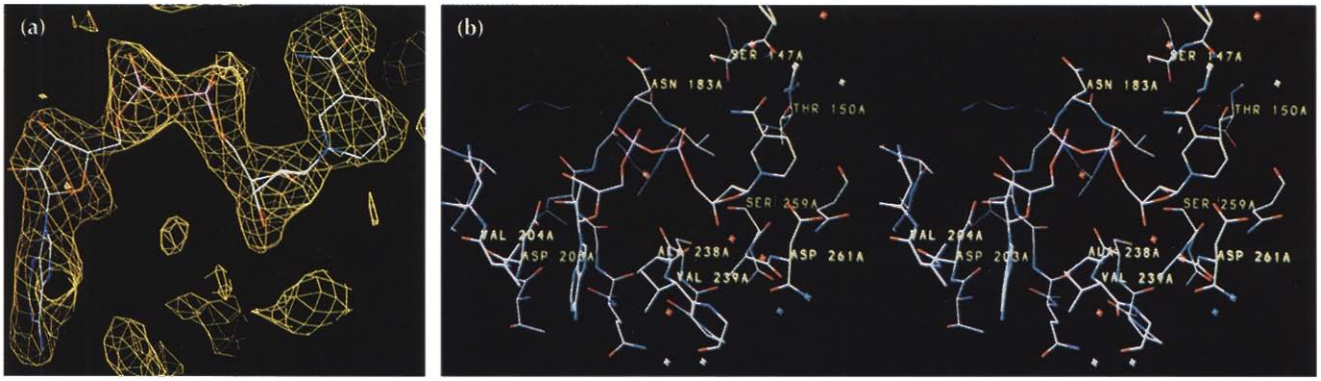

Fig. 7. (a) The positive difference electron density for the binary complex of LeuDH with NAD^+ in yellow and contoured at 1.7σ above the mean, together with the fitted model of NAD^+ shown in atom colours. **(b)** Stereo representation of NAD^+ bound to LeuDH. Residues that interact with the dinucleotide are labelled.

the side-chain carboxyl group of an acidic residue at the C terminus of βh (Asp203), which in turn forms a hydrogen bond to the main-chain amide nitrogen of a residue in the glycine-rich turn that lies between the first β-strand of the domain (βg) and the dinucleotide-binding helix, α7 [21]. The adenine ring binds in a pocket delineated by the side chains of Gln179, Val204, Pro223, Ala238, Val239 and the main-chain atoms of Gly180. The main-chain amide nitrogen of Asn183 forms a hydrogen bond to one of the adenine phosphate oxygens. The side chain of Asn183 adopts a different conformation to that seen in the free enzyme and forms interactions with the pyrophosphate. The 2′-hydroxyl of the nicotinamide ribose makes a hydrogen bond to the side chain of Asp261, the 3′-hydroxyl interacts with the main-chain carbonyl of Ala238, and the side chain of Ser259 forms a hydrogen bond to the ring oxygen of the nicotinamide ribose. The hydrogen-bonding pattern is completed by interactions between the side chains of Thr150 and Ser147 with the carboxyamide moiety of the nicotinamide ring, which leads to a *syn* conformation for the glycosidic bond between the nicotinamide ring and its associated ribose. Thus, the 4-*pro-R* hydrogen of the nicotinamide ring is buried against the enzyme surface, allowing the 4-*pro-S* hydrogen to be involved in the hydride-transfer step, explaining the stereospecificity seen in LeuDH [3]. GluDH shows an identical stereospecificity to LeuDH [22] and the binding of the dinucleotide to domain II of GluDH bears a remarkable resemblance to that described above for LeuDH. However, there are differences in the stabilization of the adenine ribose. In GluDH, the adenine ribose hydroxyls form hydrogen bonds to the main chain in the glycine-rich turn and to an asparagine residue carried on an extra loop in GluDH [16]. Furthermore, in GluDH, Arg285 from this extra loop forms a salt bridge with the pyrophosphate moiety of the cofactor. In LeuDH, this loop is missing and the stabilization of the pyrophosphate involves interactions with the side chain of Asn183. Interestingly, the α-carbon of Asn183 in LeuDH is structurally equivalent to that of Asn240 in GluDH. However, in GluDH the side chain of this residue adopts a different conformation and forms a hydrogen bond to the oxygen of the carboxyamide of the nicotinamide ring, with a further hydrogen bond to the nitrogen of the carboxyamide coming from Thr209. In LeuDH, Thr150 provides an equivalent interaction to that of Thr209 in GluDH, stabilizing the nitrogen of the carboxyamide, but the different conformation of Asn183 (compared with Asn240 in GluDH) leaves its role in hydrogen bonding to the carboxyamide oxygen to be fulfiled by Ser147.

Domain motion

Previous work on the structure of GluDH has shown that the enzyme's two domains can adopt a number of different conformations, which range from an 'open' form, required for substrate binding, to a 'closed' form, necessary for catalysis [12]. This motion can be described as a rigid-body rotation of some 14° about an axis lying between the two domains. As this crystal form of LeuDH contains a dimer in the asymmetric unit, we have been able to compare the structures of the two crystallographically independent subunits. As expected, they are largely similar to each other, with the main difference being the relative orientations of the two domains in each subunit. Superimposing the two subunits results in the α-carbon atoms in domains I (residues 1–136, 333–364) and domains II (residues 137–332) overlapping with an rms deviation of 0.17 Å and 0.35 Å, respectively. However, if the two subunits are superimposed on domain I, then the domains II of each subunit are displaced relative to one another (Fig. 8). In its simplest terms, this displacement can be described as a screw axis rotation about an axis chosen such that the translation along the chosen axis is minimized [23]. For LeuDH, the difference in the orientation of the two domains in the two subunits can be described as a rigid-body rotation of 5.4°, about an axis which lies close to the α-carbons of residues 68, 72, 134, 297, 329 and 335 and which lies approximately between the two domains, combined with a translation of 0.1 Å along this axis. Thus, in LeuDH, subunit A adopts a conformation which is similar to the open free enzyme structure of GluDH, whereas subunit B adopts a conformation in between the open and closed forms of GluDH, implying that an equivalent conformational rearrangement to that seen in GluDH will occur in LeuDH.

Fig. 8. (a) Schematic representation of the crystallographically independent subunits A (yellow) and B (blue) of the LeuDH dimer. Subunit B has been rotated around the twofold axis of the dimer to superimpose the two subunits. The N-terminal domains can be seen to overlap, whereas for domain II in subunit B a conformational change has occurred, bringing the two domains closer together and partially closing the cleft between them. (Figure prepared using Midas Plus [42,43].)

Active site

Biochemical studies have indicated that GluDH and LeuDH share a similar mechanism. Following hydride transfer, the catalytic cycle is thought to proceed through the creation of an imino acid intermediate. This intermediate is then attacked by a water molecule whose nucleophilicity is enhanced by proximity to a lysine residue with a low pK_a to produce a carbinolamine, which, in turn, breaks down to form the oxo-acid [24,25]. Structural studies on clostridial GluDH have identified residues that are thought to play a major role in the catalytic cycle [12] and a comparison of the active site of GluDH and the equivalent area in LeuDH shows that they share a similar overall architecture and contain a number of identical residues. Specifically, five glycine residues (90, 91, 122, 123 and 376) contribute to the shape of the GluDH active site and these are all conserved in LeuDH (as glycines 41, 42, 77, 78 and 290). Residues implicated in the catalytic mechanism of GluDH include Lys113, which binds the 1-carboxyl group of the glutamate substrate, Asp165, which has been proposed to be involved in proton transfer to and from the glutamate during catalysis, and Lys125, which has a low pK_a and is thought to enhance the nucleophilicity of an essential water molecule involved in the mechanism [12]. These three residues are conserved in LeuDH (Lys68, Asp115 and Lys80, respectively), and furthermore, a water molecule is present in the LeuDH structure in an equivalent position to the essential water in GluDH. The only residue in GluDH close to the catalytic centre that is modified between clostridial GluDH and LeuDH is Gln110, which is Met65 in LeuDH. However, we note that of the 24 sequences of GluDH currently available 13 contain methionine at this position. Given the overall similarity of the active site we assume that the leucine substrate of LeuDH binds in a similar fashion to the glutamate substrate in GluDH and thus we have modelled a leucine substrate into the structure of LeuDH, placing it in an equivalent position to that occupied by glutamate in GluDH (Fig. 9). As in the case of the nucleotide complex of GluDH, the distance between C4 of the nicotinamide ring and the α-carbon of the modelled leucine substrate (the partners involved in hydride transfer) is some 7 Å, a distance inconsistent with catalysis. However, we envisage that the two domains of LeuDH will close upon leucine binding, bringing the atoms involved in hydride transfer close enough for catalysis, in an analogous manner to that seen in GluDH. The ideas presented above are consistent with mutagenic studies on *B. stearothermophilus* LeuDH, which have indicated that Lys68 is located at the active site and binds to the 1-carboxyl group of the substrate [26]. Further studies on *B. stearothermophilus* LeuDH, using pyridoxal phosphate modification of lysine residues combined with mutational analysis, have shown that Lys80 has an unusually low pK_a, and have implicated this residue in the catalytic mechanism [24,27].

The model of the active site has enabled us to compare the mode of binding of the side-chain atoms of the amino acid substrates of GluDH and LeuDH. The respective substrates lie in a pocket on the enzyme surface, which has a different character in the two enzymes. In GluDH, the aliphatic 2-, 3- and 4-methylene groups of the glutamate side chain form interactions with Gly90, Ala163 and Val377, which are conserved in LeuDH (Gly41, Ala113 and Val291, respectively). However, the glutamate 5-carboxyl group makes hydrogen bonds to Lys89 and Ser380, which in LeuDH are Leu40 and Val294, two crucial substitutions that had been recognized from the earlier homology-based modelling [7]. This has the effect of making the substrate specificity pocket somewhat more hydrophobic in LeuDH and goes some way towards explaining the differential substrate specificity.

However, the complete picture is not this simple. A double mutant of GluDH, Lys89→Leu, Ser380→Val, designed to alter the substrate specificity to that of LeuDH, has been shown to be enzymatically inactive [28] and X-ray analysis has shown that a number of residues, centred around a conserved threonine (Thr193) are disordered in the mutant structure (ML Waugh, unpublished data). On close inspection of the LeuDH and GluDH structures, a subtle difference, which may explain this behaviour, is apparent in the active site. In GluDH, Thr193 forms interactions to both the substrate-binding residues, Lys89 and Ser380. Modelling studies on

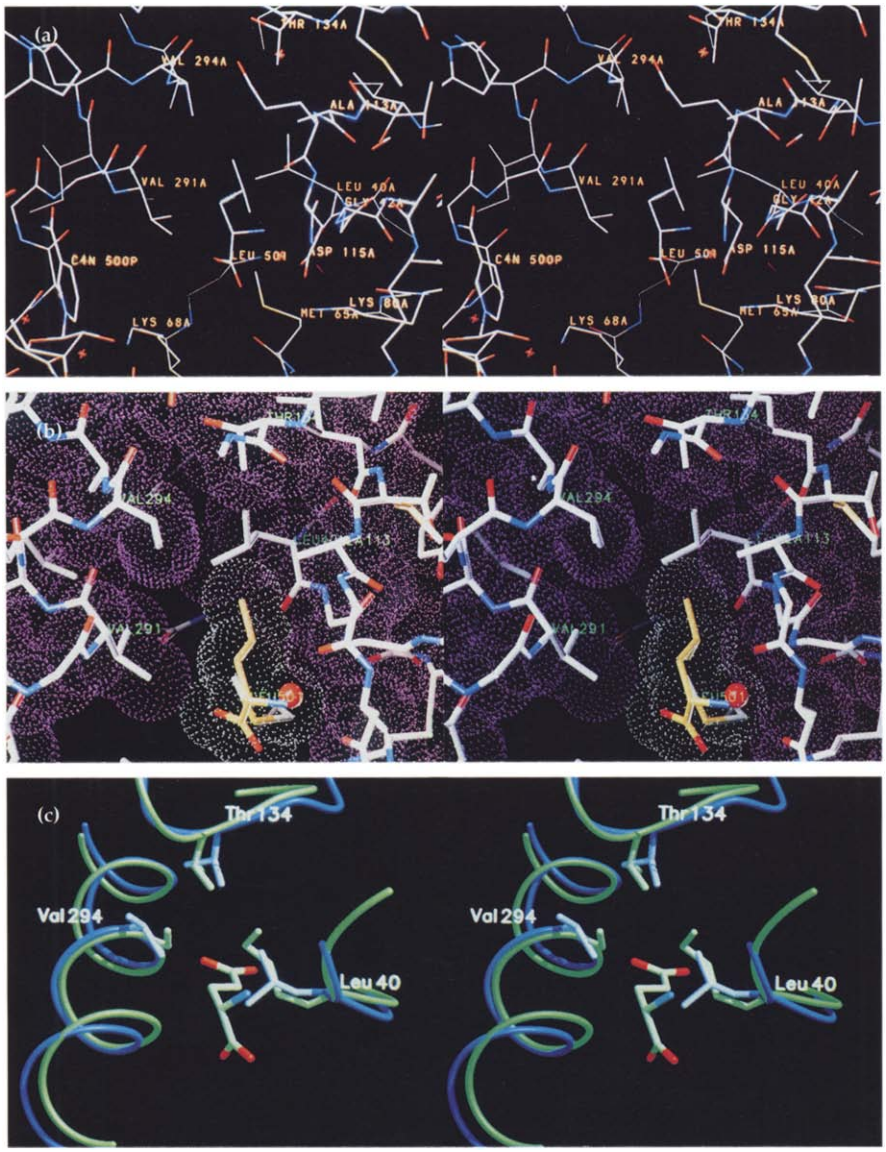

Fig. 9. Stereoviews of the proposed active site of LeuDH, with the modelled leucine substrate. **(a)** View of the overall active site, with important residues labelled. (Figure prepared using FRODO [38].) **(b)** Close-up of the side-chain specificity pocket. The polypeptide chain is shown in atom colours, the leucine substrate in yellow, and the catalytic water molecule as a red sphere. Van der Waals surfaces are shown in white for the leucine substrate and in pink for the enzyme. (Figure prepared using SYBYL [Tripos Associates Inc., St. Louis, MO].) **(c)** Schematic representation of the glutamate-binding pocket in GluDH, superimposed on the proposed leucine-binding site in LeuDH by overlapping their respective active sites. The LeuDH main chain is shown as a blue ribbon with the side chains of Leu40, Thr134 and Val294 highlighted in light blue. The GluDH main chain is shown in green with the corresponding residues, Lys89, Thr193 and Ser380, in light green. The glutamate substrate is shown in atom colours. The critical substitution Ser380→Val, required to create a more hydrophobic side-chain-binding pocket in LeuDH, cannot be made in GluDH, because of steric clashes between the valine side chain and Thr193. This view shows that the potential steric clash in LeuDH between Val294 and Thr134 is relieved by the greater distance between these two residues. (Figure prepared using Midas Plus [42,43].)

both the open and closed GluDH conformers have shown that the replacement of Ser380 by valine appears to result in a steric clash with the side chain of Thr193. In two of the three rotamers, a γ-methyl group of this valine is 2.1 Å from the γ-hydroxyl of Thr193. In the other rotamer, steric clashes occur between the γ-methyl groups of the valine and the α-carbon and main-chain carbonyl of Val377. This is consistent with the observed lack of order for these residues in the double mutant, which presumably results from an inability of the structure to accommodate this mutation. Examination of the LeuDH structure has revealed that in this enzyme the potential steric clash between the residues equivalent to Thr193 (Thr134) and Ser380 (Val294) in GluDH, is alleviated by changes in the relative position of their α-carbon atoms, caused by movement of the elements of secondary structure on which they are carried. Thus, α12 (bearing Val294) and the end of βf (bearing Thr134) move away from each other, increasing the distance between their α-carbon atoms from 5.3 Å in GluDH to 6.5 Å in LeuDH, eliminating the side-chain clash (Fig. 9). The C terminus of α12, and the loop before and after βf in LeuDH make intimate interactions about the fourfold axis with other subunits, and consequently adopt quite different folds in LeuDH and GluDH. Clearly, these changes allow the subtle re-positioning of Val294 and Thr134, which contributes to the shape of the specificity pocket. Therefore, in LeuDH, important determinants of the differential substrate specificity come not only from the substitutions of Lys89 and Ser380 in GluDH by Leu40 and Val294 in LeuDH to change the chemical nature of the substrate-binding pocket, but also from the subtle changes in the pocket shape that arise from the difference in quaternary structure. To our knowledge, this is the first reported example of a role for quaternary structure in modifying substrate specificity.

Interestingly, in the family of class I aminoacyl-tRNA synthetases, the combination of altering the chemical nature and the relative shape of the binding pocket is used as a means of discriminating between tyrosine and tryptophan in tyrosyl-tRNA synthetase (TyrRS) and

tryptophanyl-tRNA synthetase (TrpRS). Gln189 in TyrRS is replaced by Val141 in TrpRS, providing extra room for the indole six-membered ring. In concert, the relative position of a conserved aspartate residue (132 in TrpRS and 176 in TyrRS), is changed by the reorientation of the helix on which this residue is carried, in order to optimize the interactions of this residue with the respective substrate [29].

Biological implications

The rational design of enzymes for stereospecific transformations on novel substrates is a major goal in protein engineering and the investigation of enzyme families provides a route towards understanding the basic principles by which such changes may be accomplished. Glutamate, phenylalanine and leucine dehydrogenases act at the interface of carbon and nitrogen metabolism, where they catalyze the NAD(P)$^+$-linked oxidative deamination of L-amino acids to the corresponding 2-oxoacids. Sequence homology between these enzymes clearly indicates the existence of an enzyme superfamily related by divergent evolution.

Comparison of the structure of leucine dehydrogenase (LeuDH) (presented here) with that of glutamate dehydrogenase (GluDH) (the only other member of this family with a known structure), shows that they share a similar subunit structure and catalytic chemistry. However, despite this close similarity, the GluDH subunit assembles into a hexamer, whereas the LeuDH subunit forms an octamer. Comparison of these two structures shows what modifications are required to allow subunits with essentially similar architectures to assemble into an octamer (as in LeuDH) or a hexamer (as in GluDH). Interesting insights into the processes of self-assembly in these enzymes are thus revealed.

The discrimination of the amino acid substrate between these two enzymes is achieved by a combination of point mutations and subtle changes in shape in the substrate side-chain-binding pocket. Lys89 and Ser380 provide a hydrophilic pocket in GluDH, whereas in LeuDH the equivalent residues are Leu40 and Val294, which make the pocket more hydrophobic. Furthermore, the relative positions of the α-carbon atoms of this pair of residues in the two structures is subtly altered, caused by movements of the elements of secondary structure on which they are carried. These adjustments are linked to the different subunit assemblies. The involvement of quaternary structure as a partial determinant of substrate recognition offers insights into the role of quaternary structure in oligomeric enzymes. This combination of altering both the chemical nature and the relative shape of the binding pocket as a means of discriminating between amino acid substrates is similar to that observed in the aminoacyl-tRNA synthetase family.

Enzymes from the amino acid dehydrogenase superfamily are already used to produce commercial quantities of their natural substrates. A thorough understanding of the mechanisms for discriminating between the different amino acid substrates will enhance our ability to alter the specificity of these enzymes. This knowledge may find important applications in the stereospecific production or detection of novel amino acids.

Materials and methods

Crystallization

Crystals of LeuDH, isomorphous to those described previously [10], were grown using the hanging drop method of vapour diffusion. Equal portions of a protein solution at 2.5 mg ml^{-1}, in 0.1 M 2-[*N*-morpholino]ethanesulphonic acid (MES)-NaOH buffer, pH 6.0, 1 mM EDTA and a precipitant of 1.8–2.1 M ammonium sulphate in the same buffer were mixed and suspended over the precipitant solution. Bicapped tetragonal prism shaped crystals grew within two weeks to a maximum size of 0.5 mm×0.25 mm×0.25 mm. Prior to mounting, or for heavy-atom soaks, the crystals were stabilized in 2.4 M ammonium sulphate solution.

X-ray data collection

Initially, low-resolution data were collected for the native protein, and for four derivatives, which were prepared by soaking crystals in 2.5 mM K_2PtCN_4, 0.5 mM K_2PtCl_4, 2.2 mM uranyl acetate, and 0.5 mM ethylmercurithiosalicylic acid (EMTS), respectively. The data were collected at room temperature on a twin San Diego multiwire systems (SDMS) area detector, with graphite monochromated X-rays generated by a Rigaku RU200 rotating copper anode, running at 50 kV, 100 mA and with a 0.3 mm×3.0 mm cathode. The Xuong–Hamlin method of data collection was used [30,31] with ω scans of 0.12° per frame, and data collection times of 30–45 s per frame. Data were processed and merged using the SDMS software [32]. Subsequently, high-resolution data were obtained for the native protein to 2.2 Å resolution and for the K_2PtCl_4 derivative to 2.5 Å resolution at the SRS synchrotron at Daresbury (Warrington, UK). These data were collected on station PX9.5, at a wavelength of 0.912 Å, using a MAR Research imaging plate system, with 1.2° rotations per image, again at room temperature. Data for a crystal soaked in 3 mM NAD^+ were collected on station PX7.2 at the SRS, with a wavelength of 1.488 Å, a MAR Research imaging plate and 1.3° rotations per image. All SRS data were processed using the MOSFLM package [33] and other CCP4 programs [34]. Data collection statistics are shown in Table 1.

Multiple isomorphous replacement (MIR) phasing

Using the initial SDMS area detector data, the Patterson function of the K_2PtCl_4 derivative was readily interpretable and so data to high resolution were collected on this derivative. The heavy-atom positions were refined using the program MLPHARE [35] and a preliminary set of protein phases were calculated, which were used to produce difference Fouriers on the other three derivatives. All four derivatives were then refined and MIR phases calculated, to give an overall figure

Table 1. Data collection statistics.

Data set*	Detector†	Wavelength (Å)	Resolution (Å)	No. of reflections measured	No. of reflections unique	Completeness (%)	R_{merge}‡	MFID§	No. of sites	Phasing power# centric	Phasing power# acentric	R_{Cullis}** centric	R_{Cullis}** acentric	Cell dimensions (Å) a=b	Cell dimensions (Å) c
NA1	SDMS	1.5418	2.5	127180	34098	86.7	0.116	–	–	–	–	–	–	137.9	121.4
NA2	MAR	0.912	2.2	190002	57499	99.8	0.053	–	–	–	–	–	–	138.4	121.3
HG1	SDMS	1.5418	4.0	16454	13945	72.5	0.090	0.201	6	0.63	0.73	0.89	0.93	138.1	120.9
UO1	SDMS	1.5418	6.0	9422	5093	83.2	0.054	0.130	8	1.17	1.44	0.69	0.81	137.8	121.2
PT1	SDMS	1.5418	3.2	83356	34801	91.1	0.087	0.190	10	0.95	0.97	0.76	0.85	138.1	121.1
PT2	SDMS	1.5418	6.0	18789	5176	86.6	0.103	0.193	2	1.29	–	0.68	–	138.9	119.8
PT3	MAR	0.912	2.5	97803	31404	79.3	0.053	0.195	4	1.45	1.68	0.64	0.68	138.6	121.1
NAD1	MAR	1.488	2.7	48158	21366	67.9	0.075	0.140	–	–	–	–	–	138.5	121.3

*The crystals NA2 (native), PT2 (0.5 mM K_2PtCl_4, 24 h soak) and PT3 (0.5 mM K_2PtCl_4, 12 h soak) were stabilized in 2.4 M ammonium sulphate, 0.1 M MES-NaOH buffer pH 6.0, whereas NA1 (native), HG1 (0.5 mM EMTS, 12 h soak), PT1 (2.5 mM K_2PtCN_4, 48 h soak), UO1 ($UO_2[CH_3COO]_2$, 72 h soak) and NAD1 (3 mM NAD, 48 h soak) were stabilized in 2.4 M ammonium sulphate, 0.1 M *N*,*N*-bis(2-hydroxyethyl)-2-aminoethanesulphonic acid (BES)-NaOH buffer pH 7.0. †SDMS, San Diego Multiwire Systems Area Detector; MAR, MAR Research image plate. ‡$R_{merge}=\Sigma_{hkl}|I_i-I_m|/\Sigma_{hkl}I_m$, where I_i and I_m are the observed intensity and mean intensity of related reflections, respectively. §MFID is the mean fractional isomorphous difference. #Phasing power=<F_H/lack of closure>. **R_{Cullis}=<lack of closure>/<isomorphous difference>.

of merit of 0.74 to 6 Å and 0.42 to 2.5 Å. Statistics for the heavy-atom refinement and phasing are shown in Table 1.

Phase improvement

The MIR map was subjected to 10 cycles of solvent flattening using the SQUASH program [36], with the solvent content of the unit cell set to 50%. The solvent-flattened map was then skeletonized using the BONES procedure of the O program [37]. It was immediately apparent from inspection of the map and from the structure of the BONES model that the LeuDH subunit had a very similar structure to GluDH. The α-carbon atoms were then positioned for 348 residues of a single LeuDH subunit into the SQUASH map, using FRODO [38], with the model from BONES and a model of GluDH as guides. The second subunit was then generated by rigid-body rotations of the two domains of subunit A, to place them in the electron density for subunit B. The α-carbon atoms were assigned a preliminary amino acid sequence based on a consensus sequence of the *B. stearothermophilus* and *T. intermedius* LeuDHs. Automatic addition of main-chain and side-chain atoms in the preferred rotamers was undertaken using the ProLeg procedure in O [37]. One subunit was then divided into two domains and a molecular envelope was constructed for each domain using MAMA (GJ Kleywegt and TA Jones, unpublished program). The non-crystallographic symmetry (NCS) matrices relating the two domains in each subunit were defined and improved using the programs O [37] and IMP (GJ Kleywegt and TA Jones, unpublished program). Sixty cycles of symmetry averaging, solvent flattening, histogram matching and phase combination were then undertaken using the DM protocol (K Cowtan, unpublished program). During this procedure the resolution was gradually increased to 2.2 Å and the free R-factor dropped from 0.46 to 0.24. A new model of a single subunit was then built into the averaged map, using sequence data derived from the combination of peptide sequencing, a consensus sequence from *B. stearothermophilus* and *T. intermedius* and inspection of the electron-density map. The second subunit was generated by application of the NCS and this model had a total of 364 amino acids for each subunit, and an R-factor of 0.46 (for all data in the resolution range 10–2.2 Å).

Refinement

The structure was refined using the TNT package [39], including the refinement of a scale and temperature factor for the bulk solvent following the method of Moews and Kretsinger [40]. Initially the DM model was subjected to rigid-body refinement at 6 Å, and then at 3.0 Å, splitting each subunit into two rigid bodies (residues 1–136 and 332–364 for domain I, and residues 137–331 for domain II). This reduced the R-factor to 0.38 (10–3.0 Å, all data). Positional and isotropic temperature factor refinement to 2.2 Å followed to give a first refined model with an R-factor of 0.25. As the electron density for one subunit (A) was appreciably better than that for the other (B), the initial strategy was to build subunit A and generate subunit B using the NCS. The model was subjected to several rounds of rebuilding and refinement, with OMIT maps being used as necessary to rebuild poor areas of the model. During this process the electron density for both subunits was substantially improved. In the later stages of refinement the two subunits were treated separately. Solvent molecules were added to features above 2σ in a $|F_{obs}-F_{calc}|\alpha_{calc}$ map, only where they made appropriate interactions with the protein. During the process of refinement further corrections to the nature of the side chains in the LeuDH model were made, with the sequence in both subunits always being kept identical. Further rounds of rebuilding and refinement led to a final model of 364 residues for each subunit, a total of 5520 non-hydrogen atoms, 117 water sites, an average B-factor of 46.3 $Å^2$ and an R-factor of 0.20 (all data, 56941 reflections, 10–2.2 Å). The rms bond deviation was 0.016 Å, rms angle deviation 2.6°, rms trigonal atom non-planarity 0.012 Å and the rms planar groups deviation 0.015 Å.

The coordinates for leucine dehydrogenase have been submitted, with a one year delay on release, to the Brookhaven Protein Data Bank (entry code 1LEH).

Acknowledgements: We would like to thank the support staff at the Synchrotron Radiation Source at DRAL Daresbury Laboratory for assistance with station alignment, the Wellcome Trust for provision of molecular graphics facilities and the Wolfson Foundation for a laboratory refurbishment grant. This work was supported by grants from the Biotechnology and Biological Sciences Research Council (BBSRC) and the EC Biotechnology Programme. APT is a BBSRC CASE student with the Institute of Food Research at Reading. The Krebs Institute is a designated BBSRC Biomolecular Sciences Centre.

References

1. Sanwal, B.D. & Zink, M.W. (1961) L-leucine dehydrogenase of *Bacillus cereus*. *Arch. Biochem. Biophys.* **94**, 430–435.
2. Sanwal, B.D. & Zink, M.W. (1962) The distribution & substrate specificity of L-leucine dehydrogenase. *Arch. Biochem. Biophys.* **99**, 72–77.
3. Ohshima, T., Misono, H. & Soda, K. (1978). Properties of crystalline leucine dehydrogenase from *Bacillus sphaericus*. *J. Biol. Chem.* **253**, 5719–5725.
4. Nagata, S., *et al.*, & Soda, K. (1988). Gene cloning and sequence determination of leucine dehydrogenase from *B. stearothermophilus* and structural comparison with other NAD(P)$^+$-dependent dehydrogenases. *Biochemistry* **27**, 9056–9062.
5. Ohshima, T., *et al.*, & Soda, K. (1994). The purification, characterization, cloning and sequencing of the gene for a halostable and thermostable leucine dehydrogenase from *Thermoactinomyces intermedius*. *Eur. J. Biochem.* **222**, 305–312.
6. Takada, H., Yoshimura, T., Ohshima, T., Esaki, N. & Soda, K. (1991) Thermostable phenylalanine dehydrogenase of *Thermoactinomyces intermedius*: cloning, expression and sequencing of its gene. *J. Biochem.* **109**, 371–376.
7. Britton, K.L., Baker, P.J., Engel, P.C., Rice, D.W. & Stillman,T.J. (1993). Evolution of substrate diversity in the superfamily of amino acid dehydrogenases; prospects for rational chiral synthesis. *J. Mol. Biol.* **234**, 938–945.
8. Hiragi, Y., Soda, K. & Ohshima, T. (1982). Small angle X-ray scattering studies of L-leucine dehydrogenase. *Makromol. Chem.* **183**, 745–751.
9. Lünsdorf, H. & Tsai, H. (1985). Quaternary organization of subunits in the L-leucine dehydrogenase from *Bacillus cereus*. *FEBS Lett.* **193**, 261–266.
10. Turnbull, A.P., *et al.*, & Hanson, R.L. (1994). Crystallographic and quaternary structure analysis of the NAD$^+$-dependent leucine dehydrogenase from *Bacillus sphaericus*. *J. Mol. Biol.* **236**, 663–665.
11. Baker, P.J., *et al.*, & Stillman,T.J. (1992). Subunit assembly and active site location in the structure of glutamate dehydrogenase. *Proteins* **12**, 75–86.
12. Stillman, T.J., Baker, P.J., Britton, K.L. & Rice, D.W. (1993). Conformational flexibility in glutamate dehydrogenase; role of water in substrate recognition and catalysis. *J. Mol. Biol.* **234**, 1131–1139.
13. Lee, B. & Richards, F.M. (1971). The interpretation of protein structures: estimation of static accessibility. *J. Mol. Biol.* **55**, 379–400.
14. Rossmann, M.G., Moras, D. & Olsen, K.W. (1974). Chemical and biological evolution of a nucleotide-binding protein. *Nature* **250**, 194–199.
15. Rossmann, M.G., Liljas, A., Brändén, C.-I. & Banaszak, L.J. (1975). Evolutionary and structural relationships among dehydrogenases. In *The Enzymes*. (3rd edn), (Boyer, P.D., ed), pp. 61–102, Academic Press, New York.
16. Baker, P.J., Britton, K.L., Rice, D.W., Rob, A. & Stillman, T.J. (1992). Structural consequences of sequence patterns in the fingerprint region of the nucleotide binding fold: implications for nucleotide specificity. *J. Mol. Biol.* **228**, 662–671.
17. Brändén C.-I. (1980). Relation between structure & function of α/β proteins. *Quart. Rev. Biophys.* **13**, 317–338.
18. Birktoft, J.J. & Banaszak, L.J. (1984). Structure–function relationships among nicotinamide-adenine dinucleotide dependent oxidoreductases. In *Peptide and Protein Reviews*. (Hearn, M.T.W., ed) **4**, pp. 1–46, Dekker, New York.
19. Skarzynski, T., Moody, P.C.E. & Wonacott, A.J. (1987). Structure of holo-glyceraldehyde-3-phosphate dehydrogenase from *Bacillus stearothermophilus* at 1.8 Å resolution. *J. Mol. Biol.* **193**, 171–187.
20. Abad-Zapatero, C., Griffith, J.P., Sussman, J.L. & Rossmann, M.G. (1987). Refined crystal structure of dogfish M=4=apo-lactate dehydrogenase. *J. Mol. Biol.* **198**, 445–467.
21. Wierenga, R.K., De Maeyer, M.C.H. & Hol, W.G.J. (1985). Interaction of pyrophosphate moieties with α-helices in dinucleotide binding proteins. *Biochemistry* **24**, 1346–1357.
22. You, K.-S. (1985). Stereospecificity for nicotinamide nucleotides in enzymatic and chemical hydride transfer reactions. *CRC Critical Rev. Biochem.* **17**, 313–451.
23. Gerstein, M., Anderson, B.F., Norris, G.E., Baker, E.N., Lesk, A.M. & Chothia, C. (1993). Domain closure in lactoferrin, two hinges produce a see-saw motion between alternative close packed interfaces. *J. Mol. Biol.* **234**, 357–372.
24. Sekimoto, T., Matsuyama, T., Fukui, T. & Tanizawa, K. (1993). Evidence for lysine 80 as a general base catalyst of leucine dehydrogenase. *J. Biol. Chem.* **268**, 27039–27045.
25. Rife, J.E. & Cleland, W.W. (1980). Kinetic mechanism of glutamate dehydrogenase. *Biochemistry* **19**, 2328–2333.
26. Sekimoto, T., Fukui, T. & Tanizawa, K. (1994). Involvement of conserved lysine68 of *Bacillus stearothermophilus* leucine dehydrogenase in substrate binding. *J. Biol. Chem.* **269**, 7262–7266.
27. Matsuyama, T., Soda, K., Fukui, T. & Tanizawa, K. (1992). Leucine dehydrogenase from *Bacillus stearothermophilus*: identification of active site lysine by modification with pyridoxal phosphate. *J. Biochem.* **112**, 258–265.
28. Wang, X.G., Britton, K.L., Baker, P.J., Martin, S.R., Rice, D.W. & Engel, P.C. (1995). Alteration of the amino acid substrate specificity of clostridial glutamate dehydrogenase by site directed mutation of an active site lysine residue. *Protein Eng.* **8**, 147–152.
29. Doublié, S., Bricogne, G., Gilmore, C. & Carter, C.W.Jr. (1995). Tryptophanyl-tRNA synthetase crystal structure reveals an unexpected homology to tyrosyl-tRNA synthetase. *Structure* **3**, 17–31.
30. Hamlin, R. (1985). Multiwire area X-ray diffractometers. *Methods Enzymol.* **114**, 416–452.
31. Xuong, N.H., Nielsen, C. Hamlin, R. & Anderson, D. (1985). Strategy for data collection from protein crystals using a multiwire counter area detector diffractometer. *J. Appl. Crystallogr.* **18**, 342–350.
32. Howard, A.J., Nielsen, C. & Xuong, N.H. (1985). Software for a diffractometer with multiwire area detector. *Methods Enzymol.* **114**, 452–472.
33. Leslie, A.G.W. (1992). Recent changes to the MOSFLM package for processing film and image plate data. In *Joint CCP4 and ESF-EACBM Newsletter on Protein Crystallography*, No. 26. SERC Daresbury Laboratory, Warrington, UK.
34. Collaborative Computing Project, No. 4. (1994). The CCP4 suite: programs for protein crystallography. *Acta Crystallogr. D* **50** 760–763.
35. Otwinowski, Z. (1991). Maximum likelihood refinement of heavy atom parameters. In *Proceedings of the CCP4 Study Weekend* **(DL/SCI/R32)**. SERC Daresbury Laboratory, Warrington, UK.
36. Zhang, K.Y.J. (1993). SQUASH: combining constraints for macromolecular phase refinement and extension. *Acta Crystallogr. D* **49**, 213–222.
37. Jones, T.A., Zou, J.Y., Cowan, S.W. & Kjeldgaard, M. (1991). Improved methods for the building of protein models in electron density maps and the location of errors in these models. *Acta Crystallogr. A* **47**, 110–119.
38. Jones, T.A. (1985). Interactive computer graphics: FRODO. *Methods Enzymol.* **115**, 157–171.
39. Tronrud, D.E, Ten Eyck, L.F. & Matthews, B.W. (1987). An efficient general-purpose least-squares refinement program for macromolecular structures. *Acta Crystallogr. A* **43**, 489–501.
40. Moews, P.C. & Kretsinger, R.H. (1975). Refinement of the structure of carp muscle calcium-binding parvalbumin by model building and difference Fourier analysis. *J. Mol. Biol.* **91**, 201–228.
41. Kraulis, P.J. (1991). MOLSCRIPT: a program to produce both detailed and schematic plots of protein structures. *J. Appl. Crystallogr.* **24**, 946–950.
42. Ferrin, T.E., Huang, C.C., Jarvis, L.E. & Langridge, R. (1988). The MIDAS display system. *J. Mol. Graphics* **6**, 13–27.
43. Huang, C.C., Pettersen, E.F., Klein, T.E., Ferrin, T.E. & Langridge, R. (1991). Conic: a fast renderer for space-filling molecules with shadows. *J. Mol. Graphics* **9**, 230–236.

Received: **13 Apr 1995**; revisions requested: **2 May 1995**; revisions received: **17 May 1995**. Accepted: **5 Jun 1995**.